Biochemistry

 Volume 36, Number 18 May 6, 1997

Accelerated Publications

Quantitative Determination of Conformational, Dynamic, and Kinetic Parameters of a Ligand-Protein/DNA Complex from a Complete Relaxation and Conformational Exchange Matrix Analysis of Intermolecular Transferred NOESY†

Hunter N. B. Moseley,‡ Weontae Lee,§ Cheryl H. Arrowsmith,|| and N. Rama Krishna*,‡

Department of Biochemistry and Molecular Genetics and Comprehensive Cancer Center, University of Alabama at Birmingham, Birmingham, Alabama 35294-2041, Department of Biochemistry, College of Science, Yonsei University, Seoul, 120-749 Korea, and Division of Molecular and Structural Biology, Ontario Cancer Institute and Department of Medical Biophysics, University of Toronto, Toronto, Ontario, Canada M5G 2M9

Received January 31, 1997; Revised Manuscript Received March 19, 1997⊗

ABSTRACT: We report a quantitative analysis of the ^{13}C-edited intermolecular transferred NOESY (inter-TrNOESY) spectrum of the trp-repressor/operator complex (trp-rep/op) with [ul-^{13}C/^{15}N]-L-tryptophan corepressor using a computer program implementing complete relaxation and conformational exchange matrix (CORCEMA) methodology [Moseley et al. (1995) *J. Magn. Reson. 108B*, 243−261]. Using complete mixing time curves of three inter-TrNOESY peaks between the tryptophan and the Trp-rep/op, this self-consistent analysis determined the correlation time of the bound species ($\tau_B = 13.5$ ns) and the exchange off-rate ($k_{off} = 3.6$ s^{-1}) of the corepressor. In addition, the analysis estimated the correlation time of the free species ($\tau_F \sim 0.15$ ns). Also, we demonstrate the sensitivity of these inter-TrNOESY peaks to several factors including the k_{off} and orientation of the tryptophan corepressor within the binding site. The analysis indicates that the crystal structure orientation for the corepressor is compatible with the solution NMR data.

The *Escherichia coli* trp-repressor is a DNA-binding protein that functions in gene regulation. The apo-repressor is a homodimer of two 107-residue monomers. The holo-repressor has two L-tryptophan corepressor molecules which bind in a noncooperative manner to two specific binding pockets in the dimer interface. Upon binding, the two L-tryptophans bring about an allosteric transition in the nearby helix−turn−helix DNA binding motif. This transition consists of stabilizing the second helix of the helix−turn−helix motif and shifting it into a better position for interaction with its DNA operator (Arrowsmith et al., 1991; Czaplicki et al., 1991; Zhao et al., 1993). The minimal operator is an 18 base pair consensus sequence which binds the Trp-repressor with a 1:1 stoichiometry (Bennett & Yanofsky, 1987; Haran et al., 1992). Two Trp-repressors can bind in a tandem fashion to operator sequences (2:1 stoichiometry) of 33 base pairs or longer (Kumamoto et al., 1987; Liu & Matthews, 1993; Sutton et al., 1993). Trp operators are found in five operons in *E. coli* involved in tryptophan synthesis, metabolism, and transport (TrpEDCBA, aroH, aroL, TrpR, and mtr) including the Trp operon (TrpEDCBA), one of the classic examples of gene regulation (Squires et al., 1975; Sarsero et al., 1991). X-ray crystal-

† Supported by NSF Grant MCB-9630775, NCI Grant CA-13148, and NCI of Canada (C.H.A.).

* To whom correspondence should be addressed. A copy of the CORCEMA program may be obtained from this author.

‡ University of Alabama at Birmingham (UAB), Birmingham, AL.

§ Yonsei University, Seoul, Korea.

|| University of Toronto, Toronto, Ontario, Canada.

⊗ Abstract published in *Advance ACS Abstracts,* April 15, 1997.

S0006-2960(97)00242-0 CCC: $14.00

lographic structures of the apo- and holo-repressor, and holo-repressor/operator complexes are available as are the NMR structures of the apo-repressor/operator complex (Otwinowski et al., 1988; Arrowsmith et al., 1991; Zhao et al., 1993; Lawson & Carey, 1993; Zhang et al., 1994). Most recently, a NOESY analysis based on distance geometry/simulated annealing has been published that describes the orientation of the corepressor within the binding pocket (Ramesh et al., 1996). In the current study, we report a study of the corepressor orientation within the binding pocket from a complete relaxation and conformational exchange matrix (CORCEMA)[1] analysis of NOESY intensities.

The transferred NOESY (TrNOESY) experiment is a powerful tool for studying the conformations of ligands reversibly binding to large macromolecules (Ni, 1994, and references cited therein; Moseley et al., 1995, and references cited therein). This experiment uses the reversible binding of ligands in solution to sense their bound conformation and bound environment (active site). The recorded TrNOESY spectrum contains information on both free and bound ligand conformations and environments. Under favorable conditions, environmental information may include receptor molecule conformations. In general, the cross peaks in the TrNOESY spectrum reflect magnetization transfer occuring from chemical exchange as well as from intra- and intermolecular dipolar relaxation. Recent studies have identified and characterized a number of factors critical in TrNOESY analysis such as finite off-rates (Lee & Krishna, 1992; Ni, 1992; London et al., 1992; Lippens et al., 1992; Moseley et al., 1995), ligand−protein cross relaxation (London et al., 1992; Zheng & Post, 1993; Moseley et al., 1995, Curto et al., 1996), protein-mediated spin diffusion (Ni & Zhu, 1994; Moseley et al., 1994; Jackson et al., 1995; Moseley et al., 1995), motions in the active site (Moseley et al., 1995), and intermolecular NOESY contacts (Moseley et al., 1995; Curto et al., 1996).

Intermolecular TrNOESY (inter-TrNOESY) contacts between a reversibly binding ligand and the protein residues in the active site are observable under favorable conditions (James, 1976; Anglister et al., 1990; Curto et al., 1996). Such contacts provide direct information on residue orientation within the binding pocket (Curto et al., 1996). Because the spectral intensities reflect cross relaxation in multiple conformations and the exchange between these conformations, quantitative analysis should take these factors into account. CORCEMA methodology directly incorporates multiple conformations and their exchange (Moseley et al., 1995; Jackson et al., 1995; Curto et al., 1996), allowing for a quantitative analysis of multiconformational NOESY data.

Lee et al. (1995) assigned the ^{13}C-edited inter-TrNOESY contacts between the trp-repressor/operator complex (trp-rep/op) with [ul-^{13}C/^{15}N]-L-tryptophan. Due to slow exchange on the chemical shift scale, both free and bound corepressor signals are observed, including some exchange-mediated NOESY peaks (Choe et al., 1991; Lee & Krishna, 1992; Curto et al., 1996). Here, we used a computer program which implements the CORCEMA methodology to analyze the inter-TrNOESY data to see if they are compatible with the orientation of the corepressor present in the crystal structure (Otwinowski et al., 1988). As part of this analysis, we determined the corepressor exchange off-rate ($k_{off} = 3.6$ s^{-1}) and the correlation time of the bound corepressor ($\tau_B =$ 13.5 ns). Furthermore, we demonstrate the sensitivity of the TrNOESY to changes in the orientation of the corepressor and the binding pocket itself.

MATERIALS AND METHODS

NMR Experiments. The NMR sample consisted of 1 mM apo Trp-repressor dimer, 4 mM [ul-^{13}C/^{15}N]-L-tryptophan, and 1 mM double-stranded DNA. Lee et al. (1995) described the sample preparation for the experiments, as well as the experimental techniques including ^{13}C-edited NOESY. In our analysis, we used three cross peaks representing contacts between (A) the free L-tryptophan corepressor H2 (Hδ) to Thr$^{44}\gamma$ methyl (free and bound), (B) the bound L-tryptophan corepressor H2′ (Hδ′) to Thr$^{44}\gamma$ methyl (free and bound), and (C) the bound L-tryptophan corepressor H7′ (Hζ2′) to Thr$^{81}\gamma$ methyl (free and bound). The Trp-rep/op signals are dominated by the bound component but still overlap with the free component. Full-mixing time curves for all three contacts came from a series of ^{13}C-edited 2D TrNOESY experiments performed at 45 °C in D_2O on a Varian Unity600 spectrometer at 50, 100, 150, 200, 400, and 800 ms mixing times. The 50 ms point of the H2−Thr$^{44}\gamma$ contact was left out of the data set due to an experimental artifact. We normalized the cross peaks with respect to the more intense cross peaks at 100, 150, 200, and 400 ms mixing times for all three contacts (Lian et al., 1994).

CORCEMA Calculations. We developed a computer program (in the C language) called CORCEMA which solves the solution of a matrix differential equation (eq 1) for coupled magnetizations. It computes the NOESY intensity spectrum (eqs 2 and 3) for a given multiconformational-structural model (dynamic structure).

$$-\frac{d\mathbf{M}}{dt} = \mathbf{D}\,(\mathbf{M}-\mathbf{M}_0) \tag{1}$$

$$\mathbf{I}(\tau) = e^{-D\tau}\mathbf{I}(0) \tag{2}$$

$$\mathbf{D} = \mathbf{R} + \mathbf{K} \tag{3}$$

In these equations, **M** and $\mathbf{M}_0$ are the magnetization vector and its equilibrium value. **I**(τ) is the intensity matrix at mixing time τ. **D** is the dynamic matrix which is a sum of the relaxation rate matrix **R** and the exchange rate matrix **K**. Details of this implementation are given in Moseley et al. (1995). One part new in this implementation is the use of a Lipari and Szabo (1982a,b) order parameter S^2 and internal rotational correlation time to account for the effects of internal motions on internal and external methyl cross relaxation. We used the order parameter S_iS_j in an empirical manner to describe the NOESY contact between hydrogens i and j (Baleja et al., 1990). For internal methyl calculations, S_iS_j is set to 0.25 as calculated for internal methyl cross relaxation due to angular dependence (Dellwo & Wand, 1993). For external methyl calculations (i.e., CH_3-CH_3 and CH_3-H contacts), methyl hydrogens have S_i set to a given value. All other hydrogens have S_i set to 0.85 as inferred

[1] Abbreviations: CORCEMA, complete relaxation and conformational exchange matrix; NMR, nuclear magnetic resonance; NOESY, nuclear Overhauser effect spectroscopy; NOE, nuclear Overhauser effect; TrNOESY, transferred NOESY; inter-TrNOE, intermolecular transferred NOE; inter-TrNOESY, intermolecular transferred NOESY; trp-rep/op, trp-repressor/operator complex.

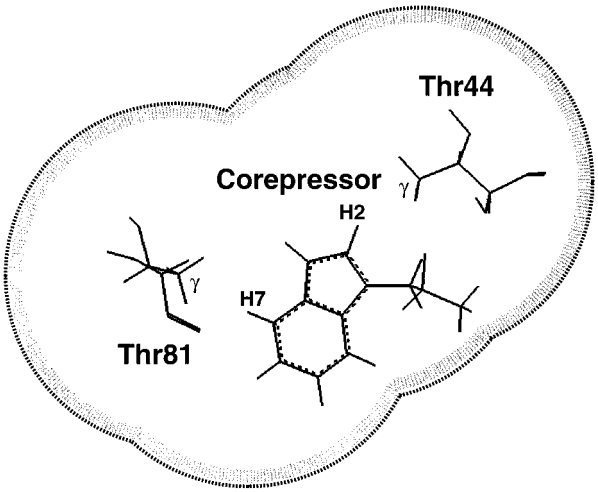

FIGURE 1: Schematic diagram showing the corepressor and the Thr44 and Thr81 residues giving rise to the inter-TrNOESY peaks used in the study. All trp-rep/op hydrogens enclosed by the four overlapping spheres centered on the methyl carbons of Thr44 and Thr81 and the H2 and H7 hydrogens of the corepressor are explicitly included in the CORCEMA analysis (they are not shown in this figure). The shaded area represents a 1 Å shell which contains hydrogens with a leakage factor of 5.0 s^{-1} to reflect interactions with trp-rep/op hydrogens outside the shell.

from an average of the S^2 for interresidue H−H contacts from Palmer and Case (1992). Therefore, the external methyl part of the order parameter is a parameter to be optimized. The internal correlation time was set to 0.005 ns [estimated for side chain values from Palmer and Case (1992)].

To analyze the data, we used a two-state model consisting of free and bound states representing free and bound conformations of the interacting species. The bound state consists of the corepressor and residues from the protein and DNA in and around the binding pocket with their coordinates obtained from the 1TRO pdb crystal structure entry (Otwinowski et al., 1988). Water molecules are excluded. The free state consists of the corepressor and the binding pocket in their uncomplexed state, but with the same conformations. To account for direct and indirect effects (spin diffusion), the binding pocket explicitly includes all hydrogens within radius r from each participating hydrogen in the NOE pair. This is represented by four overlapping spheres of radius r shown in Figure 1. All hydrogens in the binding pocket were given a uniform leakage factor of 0.1 s^{-1} to account for dissolved paramagnetic oxygen effects (strictly speaking, the tryptophan $^{13}C-^{1}H$ relaxation should also be incorporated in a more rigorous approach). However, hydrogens in the outer 1.0 Å shell were given a large leakage factor (5.0 s^{-1}) to simulate the dipolar relaxation leakage pathways of these shell hydrogens with the rest of the trp-rep/op. This way, the dimensions of the CORCEMA matrix were kept relatively small and manageable while accurately accounting for the effects of various hydrogens around the binding pocket and the leakage effects of the macromolecular lattice. The K_D was set to 10^{-5} M (Lee et al., 1995). We used the τ_F and τ_B, k_{off}, external methyl S, and free leakage factor as parameters for optimization. All computations were performed on an SGI Indigo2 workstation with R4400 150MHz chip running IRIX 5.3 and an SGI Indigo2 workstation with R4000 100MHz chip running IRIX 6.2.

Powell's Minimization. The first characteristic of optimization methods is the use of an overall fitness test or "energy" of the system for comparing different sets (or vectors) of parameters. We used an R factor calculation (Xu et al., 1995) between calculated and experimental peak intensities as the energy function (eq 4).

Table 1: Optimized Parameter Fits Using Powell Minimization with 5.0 Å Radius Sphere

model conditions	R factor	external methyl S_i	k_{off} (s^{-1})	τ_B (ns)	τ_F (ns)	free leakage factor (s^{-1})
normal conditions[a]	0.142	0.425	3.67	13.28	0.151	1.23
$k_{off} = 35.0$[a]	0.321	0.446	35.0	13.90	0.192	3.00[b]
$k_{off} = 0.35$[a]	0.303	0.410	0.35	13.73	0.001[c]	0.00[c]
Trp $\chi_2 = 112°$	0.280	1.000[b]	10.0[b]	5.00[c]	0.500[b]	3.00[b]
Trp $\chi_2 = 72°$	0.154	0.628	3.83	9.79	0.159	1.52

[a] This model has a $\chi_2 = 92°$. [b] The value is at the upper limit set for the parameter. [c] The value is at the lower limit set for the parameter.

$$R\text{ factor} = \sqrt{\frac{\sum W_i\left(\frac{I_{exp,i}}{I_{exp\_ref}} - \frac{I_{calc,i}}{I_{calc\_ref}}\right)^2}{\sum W_i\left(\frac{I_{exp,i}}{I_{exp\_ref}}\right)^2}} \quad (4)$$

In this equation, $I_{exp,i}$ and $I_{calc,i}$ refer to experimental and calculated intensities for peak i. W_i is the weighting for peak i which we set to 1 for all i. $I_{exp\ ref}$ and $I_{calc\ ref}$ are the corresponding normalization constants previously described. The second characteristic is the picking of new vectors to test. Optimization methods differ in their method of choosing new test vectors. We wrote a version of the Powell's minimization method based upon the version in *Numerical Recipes in C* (Press et al., 1992). The algorithm does a stepwise line minimization by bracketing the minimum and using Brent's method to minimize in one linear direction in vector space. This is repeated for a group of directions starting with a set of unit vectors. The algorithm then updates the directions and repeats the process until a convergence limit is reached. We reparameterized the vector components (p) in the following form (eqs 5 and 6) to allow a continuous range between infinities (p_i) to map to a finite allowable range for the parameters (p_f) within a lower bound L and upper bound U.

$$p_i = \ln\left(\frac{p_f - L}{U - p_f}\right) \quad (5)$$

$$p_f = L + \frac{(U - L)e^{p_i}}{1 + e^{p_i}} \quad (6)$$

This smooths the error surface and prevents abrupt boundary conditions that arise from using finite ranges directly. For exponential ranges, the vector parameter is the base-10 fractional exponent of the value.

RESULTS

Exchange Rate Effects. Figure 2 shows a panel of graphs displaying intensity *versus* mixing time for the three inter-TrNOESY contacts. The solid circles represent the experimental NOEs. The vertical error bars represent ±0.0138 in experimental error corresponding to 10% error for the most intense peak H7′−Thr81γ at 150 ms. The solid line represents the best optimized fit using Powell's minimization.

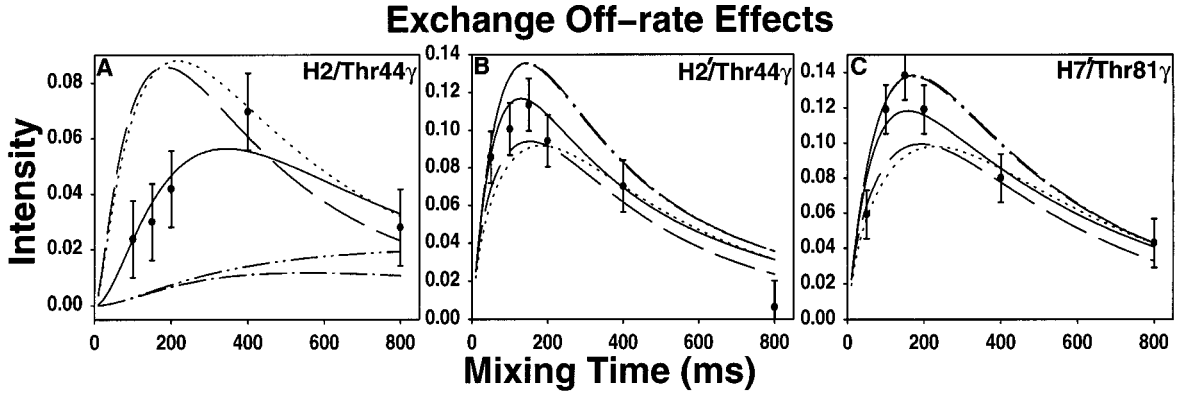

FIGURE 2: Sensitivity of the inter-TrNOESY to exchange off-rate (k_{off}). The solid circles with error bars are the experimentally derived NOEs. The solid line is the fully optimized curve. The dotted line is the unoptimized calculation with the $k_{off} = 35.0$ s^{-1}. The dashed line is the optimized calculation with the $k_{off} = 35.0$ s^{-1}. The dashed-dot line is the unoptimized calculation with the $k_{off} = 0.35$ s^{-1}. The dashed-dot-dot line is the optimized calculation with the $k_{off} = 0.35$ s^{-1} (ovelaps with other lines in graphs B and C). All curves used a 5.0 Å radius model with leakage shell.

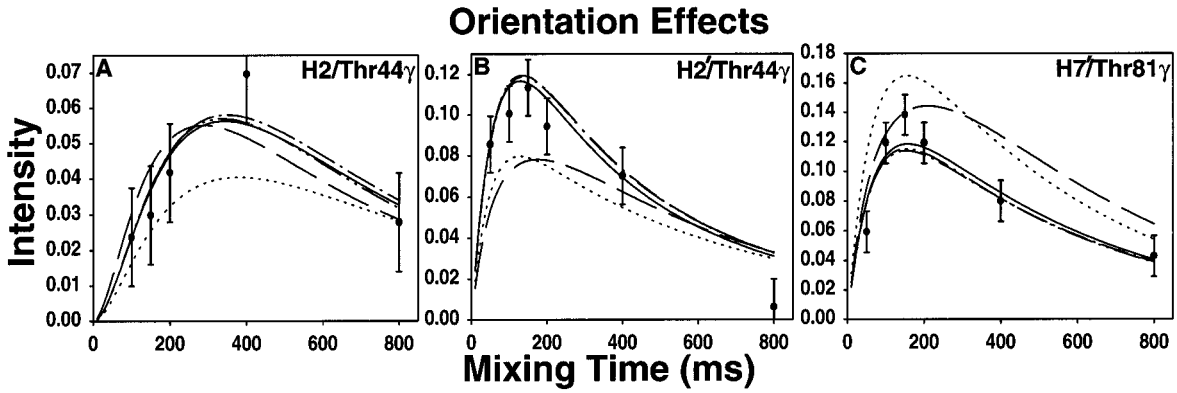

FIGURE 3: Sensitivity of the inter-TrNOESY to orientation of the corepressor in the binding pocket. The solid circles with error bars are the experimentally derived NOEs. The solid line is the optimized curve using the crystal structure orientation for the corepressor ($\chi_2 = 92°$). The dotted line is the unoptimized calculation with the corepressor $\chi_2 = 112°$. The dashed line is the optimized calculation with the corepressor $\chi_2 = 112°$. The dashed-dot line is the unoptimized calculation with the corepressor $\chi_2 = 72°$. The dashed-dot-dot line is the optimized calculation with the corepressor $\chi_2 = 72°$ (ovelaps with other lines in graphs B and C). All curves used a 5.0 Å radius model with leakage shell.

CORCEMA calculations for this best fit explicitly included all hydrogens in the binding site within a 5.0 Å radius as shown in Figure 1. This line agrees with the experimental values rather well with an *R* factor of 0.142. This optimized fit resulted in a k_{off} of 3.67 s^{-1}, a τ_B of 13.28 ns for the bound tryptophan and complex, a τ_F of 0.151 ns for the free tryptophan, a leakage factor of 1.23 s^{-1} for the free tryptophan, and an external methyl *S* of 0.425.

To test the sensitivity to k_{off}, we repeated the calculations with k_{off} fixed at 35.0 and 0.35 s^{-1}. The dashed line represents Powell's minimization fits obtained with the k_{off} fixed at 35.0 s^{-1} (an order of magnitude increase) and shows bad fits (*R* factor of 0.321) both above (graph 2A) and below (graph 2B and C) the experimental values. The fit forced the free leakage factor to its upper limit of 3.0 s^{-1} (Table 1). The dotted line represents the initial unoptimized fit using the parameters from the best fit with the k_{off} set to 35.0 s^{-1}. The dashed-dot-dot line represents the Powell's minimization fits obtained with the k_{off} fixed at 0.35 s^{-1} (an order of magnitude decrease) and shows bad fits (*R* factor of 0.303) both below (graph 2A) and above (graph 2B and C) the experimental values. Also, this fit forced the τ_F to its lower limit (0.001 ns) and the free leakage factor to zero (Table 1). The dashed-dot line represents the corresponding initial unoptimized fit using the parameters from the best fit with the k_{off} set to 0.35 s^{-1}.

Orientation Effects. Figure 3 shows a panel of graphs displaying intensity *versus* mixing time for the same three inter-TrNOESY contacts. The solid line represents the good optimized fit (Powell's minimization) previously mentioned. The dashed line represents Powell's minimization fits obtained with a 20° rotation in the χ_2 torsion angle on the tryptophan corepressor (from 92 to 112°) and shows bad fits (*R* factor of 0.280) both below (graph 3B) and above (graph 3C) the experimental values. It is the parameter values obtained from this fit that show the real gross errors. This fit resulted in a τ_B of 5.0 ns (lower limit), an external methyl *S* of 1.00 (upper limit), a k_{off} of 10.0 s^{-1} (upper limit), a τ_F of 0.5 ns (upper limit), and a free leakage factor of 3.0 s^{-1} (upper limit). Every parameter was driven to an upper or lower limit (Table 1). The dotted line represents the initial unoptimized fit with the parameters from the best fit.

The dashed-dot-dot line represents a −20° rotation in the χ_2 torsion angle (from 92 to 72°). The predicted intensities in this case are practically identical to the original set for $\chi_2 = 92°$ based on the crystallographic structure and are a reflection of much smaller changes in distances (*R* factor = 0.154). Interestingly, distance geometry analyses of these intermolecular NOESY contacts also suggest a similarly altered orientation for the corepressor being compatible with solution NMR data (Ramesh et al., 1996). However, our CORCEMA calculations show the optimized parameters are

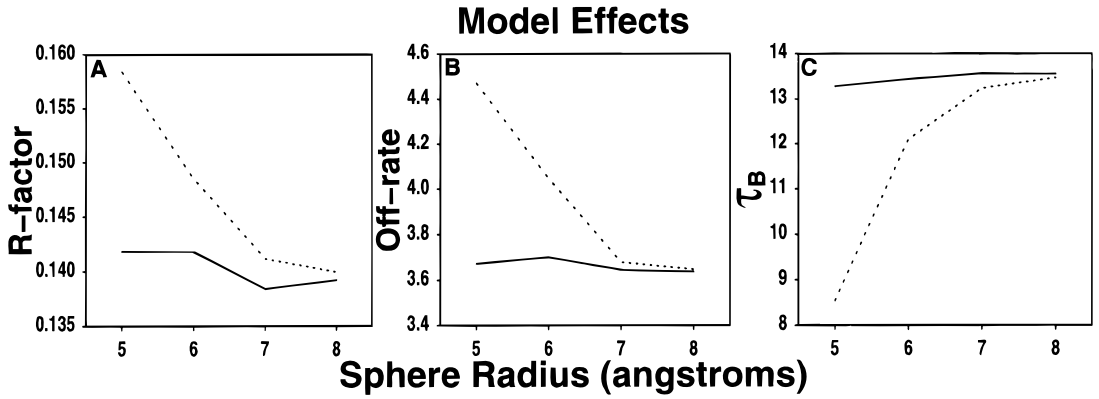

FIGURE 4: Model dependence of the optimized parameters as a function of sphere radius. The solid lines represent optimizations using a 1 Å exterior leakage shell (Figure 1). The dotted lines represent optimizations with no exterior leakage shell.

perturbed. Most noticable are the external methyl S_i of 0.628 and a τ_B of 9.79 (Table 1). The dashed-dot line represents the initial unoptimized fit with the parameters from the best fit.

Model Effects. Figure 4 represents the changes in the fits as the radius of the sphere around the binding pocket increases from 5.0 to 8.0 Å in Powell minimization fits. The solid line represents the results with an explicit leakage shell. The dotted line represents results without a leakage shell (i.e., the hydrogens in the shell have the same leakage of 0.1 s^{-1} as the other hydrogens within the overlapping spheres). In graph 4A, the *R* factor for the leakage shell model is very gradually decreasing but remains much the same as the sphere increases. The dotted line shows a dramatic decrease in the *R* factor and then asymptotically approaches the solid line as the radius increases. Graphs 4B and C represent changes in k_{off} and τ_B, respectively, as the radius of the spheres increases. A similar asymptotic behavior is observed in these graphs as in graph 4A.

DISCUSSION

Figure 2 shows big changes in the calculated NOEs when the exchange rates are perturbed from their actual values. This figure clearly demonstrates the sensitivity of this type of analysis to changes in the exchange rates when the exchange rates are comparable to the cross relaxation rates. When the exchange rates are much faster than the cross relaxation rates (fast-exchange situation), the intensities approach asymptotic values and are no longer sensitive to exchange rate changes that maintain the fast-exchange situation (Moseley et al., 1995).

Figure 4 and Table 2 show the k_{off} approaching a value of 3.6 s^{-1} as the sphere around the tryptophan binding pocket increases. This value is in excellent agreement with the direct ^{15}N-exchange-based result of 3.4 $s^{-1} \pm 0.51$ (Lee et al., 1995) and demonstrates the power of the CORCEMA approach. Also, Figure 4 and Table 2 show τ_B approaching a value of 13.5 ns at 45 °C. This value is also in excellent agreement with the direct methods value of 14.5 ± 0.9 ns at 37 °C (Shan et al., 1996). Furthermore, better accuracy of such parameters is easily obtained by increasing the number of mixing times used in the analysis. This demonstrates the usefulness and power of the CORCEMA method for obtaining the motional characteristics of a given complex of interacting molecules or a "dynamic structure."

The τ_F (∼0.15 ns) shown in Table 2 is a bit higher than expected. The increased τ_F may partly be a reflection of increased viscosity due to the presence of the 37 kDa trp-rep/op in solution (suggested by the increase in the line widths of the free corepressor signals). It may also be a reflection of the presence of nonspecific binding of the corepressor with the trp-rep/op. A low amount of nonspecific binding (less than 1% of the free) would account for the increases seen in τ_F. Furthermore, because of the relative insensitivity of inter-TrNOEs to changes in τ_F, there is inherently larger error in its value estimated through this optimization. Also, the free leakage factor (∼1.05 s^{-1} in Table 2 for 8.0 Å fit) is a bit higher than expected. Nonspecific dipolar relaxation with surface hydrogens of the Trp-rep/op due to nonspecific binding may be a contributor to this leakage. Since these studies employed ^{13}C-labeled tryptophan, dipolar relaxation with ^{13}C nuclei could make some contributions to the leakage factor as well.

Table 2: Optimized Parameter Fits Using Powell Minimization with Varied Sphere Size and Conditions

model conditions	*R* factor	external methyl S_i	k_{off} (s^{-1})[a]	τ_B (ns)[a]	τ_F (ns)[a]	free leakage factor (s^{-1})
leakage shell						
5[b]	0.142	0.425	3.67	13.28	0.151	1.23
6	0.142	0.407	3.70	13.44	0.152	1.19
7	0.138	0.393	3.65	13.56	0.151	1.04
8	0.139	0.387	3.64	13.54	0.152	1.05
no leakage shell						
5[b]	0.158	0.721	4.47	8.55	0.080	2.92
6	0.149	0.459	4.05	12.10	0.136	1.80
7	0.141	0.403	3.68	13.24	0.146	1.19
8	0.140	0.390	3.65	13.46	0.152	1.08

[a] Estimated errors are ±1.2 s^{-1} in k_{off} and ±2.0 ns in τ_B. Because of the relative insensitivity of the inter-TrNOEs to variations in τ_F, error estimates in its value are not meaningful. Further, they do not affect the results. [b] Radius length in angstrom units.

Figure 3 dramatically illustrates the sensitivity of the inter-TrNOESY to slight changes in the orientation of bound tryptophan. Both orientations caused changes in the parameters (Table 1) even when *R* factor changes were not significant for $\chi_2 = 72°$. This example illustrates that it is sometimes relatively easy to generate calculated NOE curves that show best fit with experimental data. Whether such a "best fit" is meaningful or not can only be tested from a self-consistency check, i.e., the optimized parameters (e.g., τ_B, τ_F, k_{off}, etc.) should be in reasonable agreement with independent estimates. Also, the number of "optimizable" parameters can be reduced using independent estimates. This allows the optimization to focus on interesting "optimizable"

parameters. In all, Figure 3 and Table 1 show the necessity of a self-consistentcy approach for evaluating models.

Distance geometry methods (Ramesh et al., 1996) also identified an orientation which is slightly altered. They found this orientation compatible with the NOESY data and indistinguishable from the crystal structure orientation ($\chi_2 = 92°$). This is due to nearly identical observed NOE contact distances this orientation has with the crystal structure orientation. However, other hydrogen−hydrogen distances are changed, and thus, their spin diffusion contributions to the observed NOEs are changed. CORCEMA methodology accounts for spin diffusion effects and shows additional sensitivity that identifies the $\chi_2 = 72°$ orientation as less consistent than the crystal structure orientation. Also, this example shows the potential for transferred NOESY, together with CORCEMA, to dock ligands into their binding sites. Both ligand inter-TrNOESY and intra-TrNOESY contacts would be useful for this purpose. Inter-TrNOESY contacts would sense the binding site residues directly while the intra-TrNOESY would sense them indirectly through protein-mediated spin diffusion (Curto et al., 1996). The ability of determining the bound ligand conformation, docking it into its binding site, and also determining some of its binding kinetics would be of immense benefit in structure-base drug design (Fesik, 1993). This potential makes the transfer NOESY experiment a very attractive tool indeed.

We also performed and compared simulated annealing optimizations and Powell's minimization optimizations (data not shown) under several conditions. Both methods gave nearly identical answers in almost all cases. This shows that the error surface is smooth enough to use Powell's minimization. This alleviates concerns of local minima trapping Powell's minimization. Due to the computationally expensive nature of the simulated annealing algorithm, we chose to do most of the exhaustive model testing with Powell's minimization alone.

Figures 4 shows a rigorous testing of the leakage shell model used to represent higher order interactions with distal residues. The simple fact that the nonleakage shell optimizations approached the leakage shell fits when more and more of the Trp-rep/op was incorporated validates the leakage shell model. This is further demonstrated in optimized fits where we allowed the shell leakage factor to float with the other parameters (data not shown). Every one of the fits drove the shell leakage factor to its upper limit while driving the inner-sphere leakage factor to zero as we predicted it should. In effect, the leakage shell model is simulating the leakage effects caused by the rest of the protein. Without it, the optimized parameters in small sphere fits are shifted, some dramatically (see Table 2). However, it should be noted that all hydrogens within 5−6 Å should be explicitly included. These hydrogens constitute the residues from the first and second shell of the binding pocket.

Computational efficiency becomes a factor for choosing a leakage shell model over direct incorporation of large portions of the macromolecule. Eight angstrom spheres took over 2 min for any single diagonalization (solution) of the **D** matrix. The 5 Å spheres took about 5 s. This represents a roughly 25-fold improvement in computational speed. Since the Powell optimizations required as many as 1500 diagonalizations, the use of 5 Å spheres reduced some exhaustive testing from days to hours.

CORCEMA-based full-mixing time curve analysis represents a fundamental shift in the interpretation of NOESY and transfer NOESY data. This method correctly incorporates both spin-diffusion and exchange effects involving multiple species. The method is more accurate and gives a wealth of information above traditional methods such as isolated spin-pair approximation at a single mixing time or even inital growth portion analysis based on relaxation matrix calculations. Also, this method allows for easy improvement in accuracy with the introduction of more mixing times to the curve fitting. In addition, statistical analysis of each curve can reveal obvious errors in certain mixing times.

Also, the TrNOEs at the longer mixing times, though dominated by spin diffusion, give uniquely different information from that found in the short mixing time NOEs. For example, in the presence of protein-mediated spin diffusion under fast-exchange conditions, the protein-indirect effects dominate the growth portion while the ligand-indirect effects are more pronounced in the decay portions of the intraligand TrNOEs (Jackson et al., 1995). Inter-TrNOEs at medium and long mixing times can sometimes reflect changes in the orientation of non-nearest neighbor residues at the active site (Curto et al., 1996). We suggest that NOEs at longer mixing time also be exploited in structural analyses whenever appropriate.

In fact, for typical situations in proteins, roughly 5 times as much experimental-based information is obtainable from the full-mixing time curve *versus* a single mixing time. A simple graph proof of this is the fact that it takes roughly 5 points (2 cubic splines) to adequately describe a typical NOE buildup and decay curve. This also represents the number of parameters that can be fit using the curve as data. In addition, each significant deviation in the curve represents an additional parameter or piece of information. A single mixing time or point can only be used to fit a single parameter.

In summary, this work demonstrates the use of CORCEMA methodology to determine several kinetic and dynamic parameters of the Trp-rep/op corepressor system and to show sensitivity to the orientation of the corepressor in its binding pocket. In addition, this work underscores the following findings. (1) CORCEMA methodology is a powerful tool for analyzing NOESY and TrNOESY data. (2) A wealth of information is obtainable from full-mixing time curves. (3) A self-consistent analysis of optimizable parameters, which can be supplemented by independent estimates, is required for the analysis of the TrNOESY. (4) A leakage shell model can be used in the place of full macromolecule incorporation. We conclude that CORCEMA methodology and the TrNOESY experiment have a definite place in structure-based design.

REFERENCES

Anglister, J., & Zilber, B. (1990) *Biochemistry 29,* 921.
Arrowsmith, C. H., Pachter, R., Altman, R., and Jardetzky, O. (1991) *Eur. J. Biochem. 202,* 53−66.
Baleja, J. D., Pon, R. T., & Sykes, B. D. (1990) *Biochemistry 29,* 4828−4839.
Bennett, G. N., & Yanofsky, C. (1978) *J. Mol. Biol. 121,* 179−192.
Choe, B. Y., Cook, G. W., & Krishna, N. R. (1991) *J. Magn. Reson. 94,* 387−393.
Curto E. V., Moseley, H. N. B., & Krishna, N. R. (1996) *J. Comput.-Aided Mol. Des. 10,* 361−371.

Czaplicki, J., Arrowsmith, C., & Jardetzky, O. (1991) *J. Biomol. NMR 1*, 349−361.
Dellwo, M. J., & Wand A. J. (1993) *J. Am. Chem. Soc. 115*, 1886−1893.
Fesik, S. W. (1993) *J. Biomol. NMR 3*, 261−269.
Haran, T. E., Joachimiak, A., & Sigler, P. B. (1992) *EMBO J. 11*, 3021−3030.
Jackson, P. L., Moseley, H. N. B., & Krishna, N. R. (1995) *J. Magn. Reson. 107B*, 289−292.
James, T. L. (1976) *Biochemistry 15*, 4724−4730.
Kumamoto, A. A., Miller, W. G., & Gunsalus, R. P. (1987) *Genes Dev. 1*, 556−564.
Lawson, C. L., & Carey, J. (1993) *Nature 366*, 178−182.
Lee, W., & Krishna, N. R. (1992) *J. Magn. Reson. 98*, 36−48.
Lee, W., Revington, M., Farrow, N. A., Nakamura, A., Utsunomiya-Tate, N., Miyake, Y., Kainosho, M., & Arrowsmith, C. H. (1995) *J. Biomol. NMR 5*, 367−475.
Lian, L. Y., Barsukov, I. L., Sutcliffe, M. J., Sze, K. H., & Roberts, G. C. K. (1994) *Methods Enzymol. 239*, 657−700.
Lipari, G., & Szabo, A. (1982a) *J. Am. Chem. Soc. 104*, 4559−4570.
Lipari, G., & Szabo, A. (1982b) *J. Am. Chem. Soc. 104*, 4546−4559.
Lippens, G. M., Cerf, C., & Hallenga, K. (1992) *J. Magn Reson. 99*, 268−281.
Liu, Y. C., & Matthews, K. S. (1993) *J. Biol. Chem. 268*, 23239−23249.
London, R. E., Perlman, M. E., & Davis, G. D. (1992) *J. Magn. Reson. 97*, 79−98.
Moseley, H. N. B., Curto, E. V., & Krishna, N. R. (1994) *35th Experimental NMR Conference*, p 266, Asilomar, CA.
Moseley, H. N. B., Curto, E. V., & Krishna, N. R. (1995) *J. Magn. Reson. 108B*, 243−261.
Ni, F. (1992) *J. Magn. Reson. 96*, 651−656.
Ni, F. (1994) *Prog. Nucl. Magn. Reson. Spectrosc. 26*, 517−606.
Ni, F., & Zhu, Y. (1994) *J. Magn. Reson. 103B*, 180−184.
Otwinowski, Z., Schevitz, R. W., Zhang, R. G., Lawson, C. L., Joachimiak, A., Marmorstein, R. Q., Luisi, B. F., & Sigler, P. B. (1988) *Nature 335*, 321−329.
Palmer, A. G., & Case, D. A. (1992) *J. Am. Chem. Soc. 114*, 9059−9067.
Press, W. H., Teukolsky, S. A., Vetterling, W. T., & Flannery, B. P. (1992) *Numerical Recipes in C: The Art of Scientific Computing*, 2nd ed., Cambridge University Press, Cambridge.
Ramesh, V., Syed, S. E. H., Frederick, R. O., Sutcliffe, M. J., Barnes, M., & Roberts, G. C. K. (1996) *Eur. J. Biochem. 235*, 804−813.
Sarsero, J. P., Wookey, P. J., & Pittard, A. J. (1991) *J. Bacteriol. 173*, 4133−4143.
Shan, X., Gardner, K. H., Muhandiram, D. R., Rao, N. S., Arrowsmith, C. H., & Kay, L. E. (1996) *J. Am. Chem. Soc. 118*, 6570−6579.
Squires, C. L., Lee, F. D., & Yanofsky, C. (1975) *J. Mol. Biol. 92*, 93−111.
Sutton, C. L., Mazumder, A., Chen, C. H., & Sigman, D. S. (1993) *Biochemistry 32*, 4225−4230.
Xu, Y., Sugar, I. P., & Krishna, N. R. (1995) *J. Biomol. NMR 5*, 37−48.
Zhang, H., Zhao, D., Revington, M., Lee, W., Jia, X., Arrowsmith, C. H., & Jardetzky, O. (1994) *J. Mol. Biol. 238*, 592−614.
Zhao, D., Arrowsmith, C. H., Jia, X., & Jardetzky, O. (1993) *J. Mol. Biol. 229*, 735−746.
Zheng, J., & Post, C. B. (1993) *J. Magn. Reson. 101B*, 262−270.

BI970242K